

## THERMAL TIDES IN FLUID EXTRASOLAR PLANETS

PHIL ARRAS<sup>1</sup> AND ARISTOTLE SOCRATES<sup>2</sup>

*Draft version November 2, 2018*

### ABSTRACT

Asynchronous rotation and orbital eccentricity lead to time-dependent irradiation of the close-in gas giant exoplanets – the hot Jupiters. This time-dependent surface heating gives rise to fluid motions which propagate throughout the planet. We investigate the ability of this “thermal tide” to produce a quadrupole moment which can couple to the stellar gravitational tidal force. While previous investigations discussed planets with solid surfaces, here we focus on entirely fluid planets in order to understand gas giants with small cores. The Coriolis force, thermal diffusion and self-gravity of the perturbations are ignored for simplicity. First, we examine the response to thermal forcing through analytic solutions of the fluid equations which treat the forcing frequency as a small parameter. In the “equilibrium tide” limit of zero frequency, fluid motion is present but does not induce a quadrupole moment. In the next approximation, finite frequency corrections to the equilibrium tide do lead to a nonzero quadrupole moment, the sign of which torques the planet *away* from synchronous spin. We then numerically solve the boundary value problem for the thermally forced, linear response of a planet with neutrally stratified interior and stably stratified envelope. The numerical results find quadrupole moments in agreement with the analytic non-resonant result at sufficiently long forcing period. Surprisingly, in the range of forcing periods of 1-30 days, the induced quadrupole moments can be far larger than the analytic result due to response of internal gravity waves which propagate in the radiative envelope. We discuss the relevance of our results for the spin, eccentricity and thermal evolution of hot Jupiters.

*Subject headings:* planets

### 1. INTRODUCTION

Many of the gas giant exoplanets orbiting close to their parent stars – the hot Jupiters – are observed to have radii far larger than the radius of Jupiter,  $R_J$ , implying high temperatures deep in the planetary interior (Burrows et al. 2000). A powerful internal heat source must be present in order to prevent their rapid contraction. Tidal heating is a possible solution. However, the gravitational tide synchronization and circularization timescales are much shorter than the age of the system if the tidal quality factor is comparable to that of Jupiter. Tidal heating could then power the observed radii only for a brief period, far shorter than the age of observed systems.

We propose that time-dependent thermal forcing of hot Jupiters leads to a “thermal tide” torque pushing the planet away from synchronous rotation, and possibly circular orbits. The equilibrium spin state is set by the competition between the opposing thermal and gravitational tide torques. Gravitational tide dissipation continues to operate in this torque equilibrium, implying a *steady state* heat source to power the large radii. The thermal tide torque mechanism was initially proposed by Gold and Soter (1969, GS from here on) in order to explain Venus’ slow, retrograde spin. Here, we generalize their analysis for fluid planets in which the central solid core is either non-existent or dynamically unimportant.

The existence of dynamically important thermal tide

torques in fluid planets has recently been cast in doubt (Goodman 2009 and Gu & Ogilvie 2009). These authors argue that at forcing frequencies smaller than the planet’s dynamical frequency, the quadrupole moment will be negligible due to isostatic adjustment. Furthermore, the former author asserts that the torque will push the planet toward synchronous rotation, rather than away. A careful study of the fluid motion induced by surface thermal forcing in fluid gas giant planets is needed to address the following questions: What is the direction and depth dependence of the resulting flow? What is the relevance of the concept of “isostatic adjustment” to this inherently time-dependent problem? What sets the “dynamical frequency below which the quadrupole moments become small? What is the sense of the torque (synchronous versus asynchronous)? What is the magnitude of the torque? Once these questions have been answered, the ability of thermal tide torques to promote asynchronous rotation and tidally inflated radii can then be assessed.

Here, we study the fluid flow and resulting quadrupole moments induced by thermal forcing at the surface of a gas giant planet. To isolate what we believe to be the relevant physical mechanisms, we ignore thermal diffusion, the Coriolis force and self-gravity of the perturbations, while utilizing a simplified model for the planetary structure.

The plan of this paper is as follows. In §2 we provide motivation for performing the ensuing calculations. We then describe the problem set-up and details of the background model for the fluid planet in §3. §4 reviews the relation between density perturbation and quadrupole moment, and the torque on the planet and orbit in terms of

Electronic address: socrates@ias.edu, arras@virginia.edu  
<sup>1</sup> Department of Astronomy, University of Virginia, P.O. Box 400325, Charlottesville, VA 22904-4325

<sup>2</sup> Institute for Advanced Study, Einstein Drive, Princeton, NJ 08540

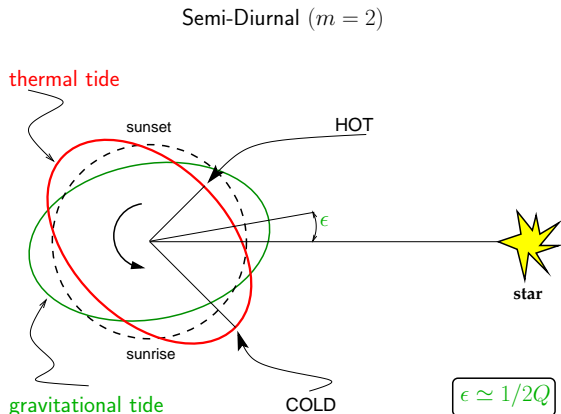


FIG. 1.— Geometry of the semi-diurnal ( $m = 2$ ) thermal and gravitational tidal density perturbations. The planet rotates counterclockwise. In order for the torque to push the planet away from synchronous spin, the density perturbation must *lead* the line joining planet and star.

the quadrupole moment. The linearized fluid equations are presented in §5. In §5.1 and 5.2 we develop analytic solutions in the zero and small, but finite, frequency limit. Numerical results to the linearized boundary value problem are presented in §5.3. In §6, the numerical results are explained in terms of the response of envelope gravity waves that are excited thermal forcing. We summarize in §8.

## 2. MOTIVATION

We begin with a brief discussion of the possible role of thermal tides for the rotation rates and radii of hot Jupiters.

Thermal forcing may induce a “bulge” which is misaligned with star-planet line (see figure 1). The misalignment is a result of thermal inertia, the tendency of maximum temperature to lag maximum heating. Since insolation is finite on the day side and zero on the night side, thermal forcing is spread over a range of harmonics. In particular, the semi-diurnal ( $m = 2$ ) component of the thermal forcing may induce a quadrupole moment in the fluid, which can then couple to stellar gravitational field. Therefore, this “thermal tidal torque” can, in principle, push the planet away from a synchronous spin state. The equilibrium spin rate is then set by a balance of the thermal tide torque, promoting asynchronous spin, and the gravitational tide torque, which acts to push the spin back toward the synchronous state. The two bulges are illustrated in figure 1.

In the asynchronous spin state set by torque equilibrium, the gravitational tide generates heat in a steady state manner. If the dissipation occurs sufficiently deep within the convective core of the planet, a thermal equilibrium will be established between (gravitational) tide heating of the core and heat loss at the radiative-convective boundary. To explain the large observed radii, the equilibrium core entropy must be much larger than that of a passively cooling planet at the same age.

The thermal tide torque is expected to deposit angular momentum mainly in the surface radiative layer. Were there no sink of angular momentum, the total angular momentum of the planet would increase indefinitely. If we again assume that gravitational tide dissipation occurs deep in the convective core, then angular momentum

must be transported between the thermal tide source region and the gravitational tide sink region. Presumably this angular momentum transport would be accomplished through (turbulent) viscous forces between neighboring fluid layers.

We estimate the importance of thermal tides in hot Jupiters by comparing the quadrupole moment induced by the thermal tide to that from dissipation acting on the gravitational tide. For the purposes of a fiducial estimate, we use the thermal tide quadrupole formula relevant for Venus by Gold & Soter (1969):

$$Q^{(\text{th})} \sim \frac{\Delta M R_p^2}{\sigma t_{\text{th}}}. \quad (1)$$

Here  $\Delta M$  is the mass down to the photospheric layer for the starlight,  $R_p$  is the planet’s radius,  $\sigma$  is the tidal forcing frequency and the thermal time of the absorbing layer is given by

$$t_{\text{th}} \sim \frac{\Delta M c_p T}{R_p^2 F_*}, \quad (2)$$

where  $c_p$  is the specific heat at constant pressure,  $T$  is the temperature, and  $F_*$  is the stellar flux. The frequency dependence in eq.1 reflects that the temperature and density perturbations in the atmosphere become small when the forcing period is short. The accuracy with which eq.1 represents a fluid atmosphere is the subject of the remainder of the paper.

The quadrupole moment induced by the stellar gravitational tide which leads to secular evolution is given by (e.g. Goldreich & Soter 1966)

$$Q^{(\text{grav})} \sim \left(\frac{h_t}{R_p}\right) \left(\frac{\sigma}{n}\right) \frac{M_p R_p^2}{Q_p} \quad (3)$$

where the height of the tidal bulge is  $h_t \sim R_p (M_*/M_p) (R_p/a)^3$ , the orbital frequency is  $n \simeq (GM_*/a^3)^{1/2}$ , the semi-major axis is  $a$ , the stellar mass is  $M_*$ , and the tidal quality factor of the planet is  $Q_p$ . Here  $\sigma \propto n - \Omega$  is proportional to the departure of the rotation rate  $\Omega$  from synchronous rotation,  $\Omega = n$ . As a fiducial value, the tidal quality factor of Jupiter is constrained to be  $Q_p \sim 10^5 - 10^6$  (Goldreich & Soter 1965; Yoder & Peale 1981).

The ratio between the thermal tide and gravitational tide quadrupole is given by

$$\begin{aligned} \frac{Q^{(\text{th})}}{Q^{(\text{grav})}} &\sim \left(\frac{n}{\sigma}\right)^2 \left(\frac{\Delta M}{M_p}\right) \left(\frac{M_p a^3}{M_* R_p^3}\right) \left(\frac{Q_p}{n t_{\text{th}}}\right) \\ &\simeq \left(\frac{n}{\sigma}\right)^2 \left(\frac{\Delta M}{10^{-8} M_p}\right) \left(\frac{M_p}{10^{-3} M_*}\right) \\ &\quad \times \left(\frac{a}{10^2 R_p}\right)^3 \left(\frac{Q_p}{10^5}\right) \left(\frac{1}{n t_{\text{th}}}\right). \end{aligned} \quad (4)$$

The fiducial estimate in eq.4 shows that thermal and gravitational tidal effects are competitive for hot Jupiters, with large departures from synchronous spin  $\sigma \sim n$  expected.

Given the equilibrium spin rate, the gravitational tide will generate heat at a rate

$$\dot{E}^{(\text{GT})} = \frac{\sigma}{m} n^2 Q^{(\text{grav})} = -\frac{\sigma}{m} n^2 Q^{(\text{th})} \quad (5)$$

$$\simeq 10^{28} \text{ erg s}^{-1} \left(\frac{\sigma}{n}\right) \left(\frac{3 \text{ days}}{P_{\text{orb}}}\right)^3 \left(\frac{Q^{(\text{th})}}{10^{-8} M_J R_J^2}\right).$$

This fiducial estimate of the heating rate is comparable, or larger than, the core cooling rates found in Arras & Bildsten (2006) for many “problem” planets, which cannot be explained by passive cooling. If this tidal heating is deposited sufficiently deep in the core, it may then prevent these planets from contracting, explaining the inflated radii of some hot Jupiters.

### 3. PROBLEM SET UP

In this section we expand the thermal and gravitational forcing terms in terms of a Fourier expansion, define the co-ordinate system used, and discuss the background planetary structure model.

#### 3.1. description of time-dependent thermal and gravitational forcing

We seek solutions to the boundary value problem describing linear response of a gaseous planet to a gravitational tidal acceleration  $-\nabla U(\mathbf{x}, t)$  and an imposed entropy perturbation,  $\Delta s(\mathbf{x}, t)$ , that results from time-dependent insolation.

Consider a planet of mass  $M_p$  and radius  $R_p$  in a circular orbit of separation  $a$  around a solar-type star of mass  $M_\star = M_\odot$ , radius  $R_\star = R_\odot$  and effective temperature  $T_\star = 5800$  K. The bolometric flux at the planet’s surface is then  $F_\star = \sigma_{\text{sb}} T_\star^4 (R_\star/a)^2$ , where  $\sigma_{\text{sb}}$  is the Stefan-Boltzmann constant. The orbital frequency is  $n = (GM_\star/a^3)^{1/2}$  and the planet’s spin frequency is  $\Omega$ . The orbital phase in the frame corotating with the planet will be denoted  $\Phi = (n - \Omega)t$ .

It is convenient to express  $U(\mathbf{x}, t)$  and  $\Delta s(\mathbf{x}, t)$  in a Fourier series in time and spherical harmonics in angle i.e.,

$$\Delta s(\mathbf{x}, t) = \sum_{\ell m} \Delta s_{\ell m}(r) Y_{\ell m}(\theta, \phi) e^{-i\sigma_m t} \quad (6)$$

and

$$U(\mathbf{x}, t) = \sum_{\ell m} U_{\ell m}(r) Y_{\ell m}(\theta, \phi) e^{-i\sigma_m t}. \quad (7)$$

The forcing frequency is then  $\sigma_m = m(n - \Omega)$ .<sup>3</sup> For  $\ell = 2$ , only  $m = \pm 2$  are allowed due to the even parity of  $U$  and  $\Delta s$ . We note that while the longitude-dependent stellar irradiation is zero on the night side and nonzero on the day side, the individual Fourier components are nonzero on both day and night sides. By adding together many Fourier components one recovers the true position-dependent flux.

Lagrangian and Eulerian variations are denoted by  $\Delta$  and  $\delta$ , respectively. The Lagrangian entropy perturbation,  $\Delta s$ , is a convenient variable to use as it varies solely due to non-adiabatic processes, here the time-dependent heating due to insolation. By contrast, the Eulerian entropy perturbations can vary due to motion parallel to a background entropy gradient, and the temperature can vary due to pressure perturbations.

<sup>3</sup> For an eccentric orbit, this expression is generalized to  $\sigma_{mk} = kn - m\Omega$  where  $k$  is an integer.

Unfortunately, the governing equations are not separable when the Coriolis force is included. Due to this complication, for simplicity, we neglect the Coriolis force. By doing so, the response for each individual spherical harmonic can be studied separately. We will suppress the subscripts ( $\ell, m$ ) where no confusion will arise.

Scalar quantities are represented as  $f(\mathbf{x}, t) = f(r) Y_{\ell m}(\theta, \phi) e^{-i\sigma t}$ , and the Lagrangian displacement vector,  $\boldsymbol{\xi}(\mathbf{x}, t)$  is expanded in the poloidal harmonics

$$\boldsymbol{\xi}(\mathbf{x}, t) = [\xi_r(r) \mathbf{e}_r + \xi_h(r) r \nabla] Y_{\ell m}(\theta, \phi) e^{-i\sigma t}. \quad (8)$$

The entropy perturbation  $\Delta s$  is related to the Lagrangian density and pressure perturbations,  $\Delta \rho$  and  $\Delta p$  respectively, via the thermodynamic relation

$$\frac{\Delta \rho}{\rho} = \frac{\Delta p}{\Gamma_1 p} + \rho_s \frac{\Delta s}{c_p}. \quad (9)$$

Here  $\Gamma_1 = (\partial \ln P / \partial \ln \rho)_s$  is the first adiabatic index,  $c_p = T(\partial s / \partial T)_p$  is the specific heat per unit mass at constant pressure, and  $\rho_s = c_p(\partial \ln \rho / \partial s)_p$  is the negative of the volume expansion coefficient at constant pressure. For an ideal gas,  $\rho_s = -1$ .

If the thermal inertia of the absorbing layer is large, then thermal diffusion can be ignored on the timescale  $\sigma^{-1}$  of the perturbation. From here on, we assume that this limit applies. Perturbations of the heat equation then take on the simple form

$$\frac{\Delta s}{c_p} = \frac{i}{\sigma} \frac{\delta \epsilon}{c_p T}. \quad (10)$$

Here  $\delta \epsilon$  is the perturbed rate of heating, per unit mass. The depth dependence of  $\delta \epsilon$  is approximated as

$$\delta \epsilon(p) = \kappa_\star F_\star \exp(-\kappa_\star p/g) \quad (11)$$

for the  $\ell = |m| = 2$  harmonics of interest. Here,  $\kappa_\star$  is the effective opacity for where starlight is absorbed, at a characteristic pressure  $g/\kappa_\star$ . The thermal time at the base of the heated layer is  $t_{\text{th}} = c_p T / \kappa_\star F_\star$ . Therefore, the imposed entropy perturbation can be written as

$$\frac{\Delta s}{c_p} = \frac{i}{\sigma t_{\text{th}}} \exp(-\kappa_\star p/g). \quad (12)$$

For semi-diurnal forcing of an asynchronously rotating planet, the stellar insolation  $\delta \epsilon$  achieves its maximum value at noon and at midnight. The entropy perturbation  $\Delta s$  then attains maxima at 3PM and 3AM, and minima at 9AM and 9PM.

The  $\ell = 2$  coefficients for the tidal potential are given by

$$U_{2m} = -\sqrt{\frac{3\pi}{10}} n^2 r^2 \quad (13)$$

for both  $m = \pm 2$ .

#### 3.2. Background Model

Hot Jupiters possess a convective core, blanketed by a thin radiative envelope at the surface (e.g. Burrows et al. 2000, Arras & Bildsten 2006). Rather than construct a model with a detailed equation of state and radiative transfer, we use a simple parametrized equation of state

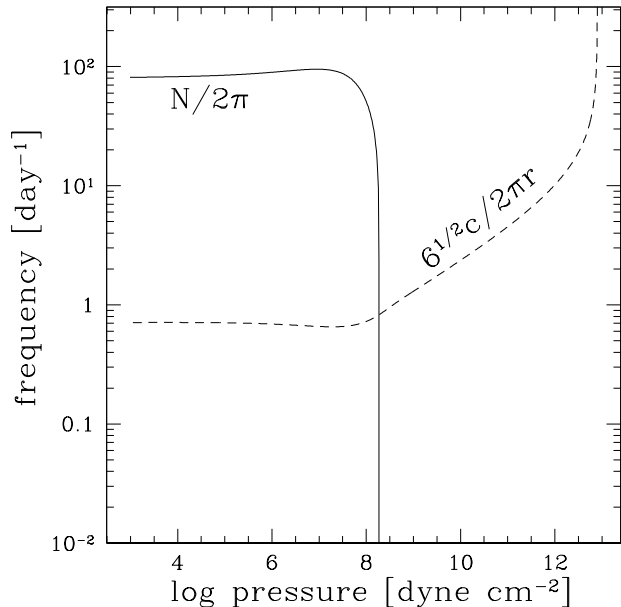


FIG. 2.— Propagation diagram showing Brunt-Vaisalla frequency ( $N$ , solid line) and Lamb frequency for  $\ell = 2$  ( $6^{1/2}c/r$ , dashed line) as a function of depth. An acoustic wave with a fixed frequency  $\sigma$  can propagate in regions where  $\sigma > N, ck_{\perp}$  and gravity waves can propagate where  $\sigma < N, ck_{\perp}$ . Here  $c$  is the adiabatic sound speed and  $k_{\perp} = \sqrt{6}/r$  is the horizontal wavenumber. The region near the surface with  $N^2 > 0$  is stably stratified, and the central region with  $N^2 \approx 0$  is neutrally stratified.

which enforces neutral stratification in the core and stable stratification with roughly constant scale height in the envelope. The equation of hydrostatic balance is integrated using

$$\rho(p) = e^{-p/p_b} \left( \frac{p}{a^2} \right) + \left( 1 - e^{-p/p_b} \right) \sqrt{\frac{p}{K_c}}. \quad (14)$$

The constants  $p_b$ ,  $K_c$  and  $a = (p_b K_c)^{1/4}$  are the pressure at the base of the radiative envelope, parameter setting the entropy of the core and the isothermal sound speed of the envelope, respectively. The factors with  $e^{-p/p_b}$  enforce a narrow transition at the radiative-convective boundary. The core compressibility is set to  $K_c = GR_J^2$ . The propagation diagram for a model with  $p_b = 100$  bar is shown in figure 2. The mass and radius are  $M_p = 0.7M_J$  and  $R_p = 1.27R_J$ . The mass of the radiative envelope is roughly  $p_b/p(r=0) = 10^{-5}$  of the planet's total mass. Though this model is simple, it accurately reproduces the gross features of more detailed models (cf. Arras & Bildsten).

To compute the sound speed we take  $\Gamma_1 = 2$  so that the core is neutrally stratified. The Brunt-Vaisalla frequency is then

$$\begin{aligned} N^2 &= -g \left( \frac{d \ln \rho}{dr} - \frac{1}{\Gamma_1} \frac{d \ln p}{dr} \right) \\ &= \frac{g}{H} \left( \frac{d \ln \rho}{d \ln p} - \frac{1}{\Gamma_1} \right) \end{aligned} \quad (15)$$

where  $g(r) = Gm(r)/r^2$  is the gravity,  $H = p/\rho g$  is the pressure scale height, and the derivative  $d \ln \rho / d \ln p$  is

computed analytically from eq. (14).

#### 4. QUADRUPOLE MOMENT AND TIDAL TORQUES

The interaction Hamiltonian, which coupled the density field of the planet to the gravitational tidal potential of the star is given by (e.g. Newcomb 1962)

$$H = \int d^3 x^* \rho^*(\mathbf{x}^*, t) U(\mathbf{x}^*, t). \quad (16)$$

Here  $\mathbf{x}^*$  and  $\rho^*$  are the position and mass density of a fluid element in the perturbed planet. The fluid position in the background planet,  $\mathbf{x}$ , and in the perturbed planet,  $\mathbf{x}^*$ , are related by  $\mathbf{x}^* = \mathbf{x} + \boldsymbol{\xi}(\mathbf{x}, t)$ , where  $\boldsymbol{\xi}$  is the Lagrangian displacement vector. Mass conservation implies  $d^3 x^* \rho^*(\mathbf{x}^*, t) = d^3 x \rho(\mathbf{x})$ , where the volume integral is performed over the background planet. Eq.(16) may then be expanded as

$$\begin{aligned} H &= \int d^3 x \rho(\mathbf{x}) U(\mathbf{x} + \boldsymbol{\xi}, t) \\ &\simeq \int d^3 x \rho(\mathbf{x}) [U(\mathbf{x}) + \boldsymbol{\xi} \cdot \nabla U(\mathbf{x}, t) + \mathcal{O}(\xi^2)]. \end{aligned} \quad (17)$$

The first term in eq. (17) corresponds to the interaction energy of the background, and can be ignored since it is independent of  $\xi$ . The second term is the interaction energy of the perturbations at linear order and is the term of interest. We ignore nonlinear terms of order  $\xi^2$  on the assumption that they are small.

To evaluate eq. (17), we expand the tidal potential in spherical harmonics (see eq.7)

$$U(\mathbf{x}, t) = -GM_{\star} \sum_{\ell m} \frac{4\pi}{2\ell + 1} \left( \frac{r^{\ell}}{D^{\ell+1}} \right) Y_{\ell m}(\pi/2, \Phi) Y_{\ell m}^*(\theta, \phi) \quad (18)$$

and define the time-dependent multipole moments of the planet

$$Q_{\ell m}(t) = \int d^3 x \rho \boldsymbol{\xi}(\mathbf{x}, t) \cdot \nabla (r^{\ell} Y_{\ell m}^*(\theta, \phi)). \quad (19)$$

Here  $D$  and  $\Phi$  are the orbital separation and phase. Integrating by parts and using the continuity equation for the perturbations

$$\delta \rho = -\nabla \cdot (\rho \boldsymbol{\xi}), \quad (20)$$

eq. (19) becomes

$$Q_{\ell m}(t) = \int d^3 x r^{\ell} Y_{\ell m}^*(\theta, \phi) \delta \rho(\mathbf{x}, t). \quad (21)$$

Hence it is the Eulerian density perturbation which is needed for the quadrupole moment.

Since  $r^{\ell} \delta \rho(\mathbf{x}, t)$  is a real quantity, and  $Y_{\ell m}^* = (-1)^m Y_{\ell, -m}$ , the moments must satisfy  $Q_{\ell m}^* = Q_{\ell, -m} (-1)^m$ . By defining  $W_{\ell m} \equiv [4\pi/(2\ell + 1)] Y_{\ell m}(\pi/2, 0)$ , the interaction Hamiltonian in eq. (16) may be conveniently expressed in terms of a sum over spherical harmonics as

$$H(D, \Phi) = -GM_{\star} \sum_{\ell m} W_{\ell m} Q_{\ell m}^*(t) \frac{e^{-im\Phi}}{D^{\ell+1}}. \quad (22)$$

The rate of change of orbital angular momentum,  $L_{\text{orb}} = GM_p M_{\star} (Ga/(M_p + M_{\star}))^{1/2}$ , and the torque on

the planet,  $\mathcal{N}$ , are then

$$\dot{L}_{\text{orb}} = -\mathcal{N} = -\frac{\partial}{\partial \Phi} H(D, \Phi). \quad (23)$$

The secular evolution of the planet-orbit system is due to the presence of quadrupole moments that are out of phase with the tidal acceleration i.e., the imaginary component of the quadrupole. The torque on the planet for a circular orbit is dominated by the semi-diurnal term with  $|m| = 2$  and forcing frequency  $2(n - \Omega)$ . The torque at this order is

$$\begin{aligned} \mathcal{N} &= 4 \left( \frac{3\pi}{10} \right)^{1/2} \left( \frac{M_p + M_\star}{M_\star} \right) n^2 \text{Im}(Q_{22}) \\ &\simeq 4n^2 \text{Im}(Q_{22}). \end{aligned} \quad (24)$$

The sign in eq. (24) is such that density perturbations which *lead* maximum heating tend to torque the planet *away* from synchronous rotation, and vice versa.

### 5. SOLUTION OF THE BOUNDARY VALUE PROBLEM

Conservation of mass and momentum, the first law of thermodynamics, and two boundary conditions are employed in order to obtain the planet's response to thermal and gravitational forcing. First we develop equations that can be solved as a boundary value problem. We then show that planet's response can be represented as a sum of eigenmodes. The governing equations below are standard and can be found in, for example, Unno et al. (1989).

Conservation of horizontal and vertical momentum are given by

$$-\sigma^2 \xi_h = - \left( \frac{\delta p / \rho + U}{r} \right) \quad (25)$$

and

$$-\sigma^2 \xi_r = -\frac{1}{\rho} \frac{d\delta p}{dr} - g \frac{\delta \rho}{\rho} - \frac{dU}{dr}, \quad (26)$$

respectively. Here  $\delta p$  and  $\delta \rho$  are the Eulerian pressure and density perturbations. We ignore the self-gravity of the perturbations for simplicity. The continuity eq. (20) may be written as

$$\frac{\delta \rho}{\rho} = -\frac{1}{r^2 \rho} \frac{d}{dr} (r^2 \rho \xi_r) + \frac{\ell(\ell+1)}{r} \xi_h \quad (27)$$

$$= -\frac{1}{r^2 \rho} \frac{d}{dr} (r^2 \rho \xi_r) + \frac{\ell(\ell+1)}{\sigma^2 r^2} \left( \frac{\delta p}{\rho} + U \right). \quad (28)$$

where we have used eq. (25). By substituting the relation between Lagrangian and Eulerian quantities i.e.,  $\Delta = \delta + \xi \cdot \nabla$ , eq. (9) becomes

$$\frac{\delta \rho}{\rho} = \frac{\delta p}{\rho c^2} + \frac{N^2}{g} \xi_r + \rho_s \frac{\Delta s}{C_p} \quad (29)$$

where  $c^2 = \Gamma_1 p / \rho$  is the adiabatic sound speed. The imposed entropy perturbations drive vertical fluid motion through buoyancy forces  $-g\rho\rho_s \Delta s / c_p$ . The vertical fluid motion in turn drives horizontal motion.

We solve the system of 3 equations (26), (28) and (29), for the three variables  $\delta p$ ,  $\delta \rho$  and  $\xi_r$ . While  $\delta \rho$  can be eliminated as well, we find that better numerical precision is achieved by keeping  $\delta \rho$  in the system of equations.

Finally, we remark on the boundary conditions. Eq.(29) is algebraic, so no boundary condition is needed as this equation can be evaluated on the boundaries. At the center of the planet, we require all variables to be finite. This implies (e.g. Unno et al. 1989; take  $\xi_r \propto r^{\ell-1}$  and  $\delta p, \delta \rho \propto r^\ell$  in eq.26)

$$\sigma^2 \xi_r = \frac{\ell}{r} \left( \frac{\delta p}{\rho} + U \right). \quad (30)$$

We present results for two different upper boundary conditions. The ‘‘standard’’ boundary condition requires that the Lagrangian pressure perturbation  $\Delta p$  vanishes (Unno et al. 1989)

$$\delta p / \rho = g \xi_r. \quad (31)$$

If the fluid perturbation is evanescent, this boundary condition is valid. We also present results for an ‘‘outgoing wave’’ boundary condition, in which wave energy propagates outward at the upper boundary (e.g. Unno et al. 1989). We implement this outgoing wave boundary condition as follows. The atmosphere above the upper boundary is idealized as isothermal, with constant  $H$ ,  $N$ ,  $g$ ,  $c$  and horizontal wavenumber  $k_\perp = \sqrt{\ell(\ell+1)} / R_p$ . In an isothermal atmosphere, the fluid variables  $\delta p / \rho, \xi_r \propto e^{bz}$  (cf. Goldreich & Kumar 1990), where  $z$  is altitude and the complex constant

$$b = \frac{1}{2H} \pm i \left[ k_\perp^2 \frac{N^2}{\sigma^2} - k_\perp^2 + \frac{\sigma^2}{c^2} - \frac{1}{4H^2} \right]^{1/2} \quad (32)$$

determines the run with height. When the argument of the square root is positive, the wave is propagating. The sign of the second order wave flux is

$$F_{\text{wave}} = \delta p \dot{\xi}_r \propto - \left( \frac{\sigma}{N^2 - \sigma^2} \right) \text{Im}(b). \quad (33)$$

We choose outgoing wave flux by choosing the appropriate sign of  $\text{Im}(b)$  to make  $F_{\text{wave}} > 0$ , given the signs of  $\sigma$  and  $N^2 - \sigma^2$ . For the propagating case, the boundary condition is enforced as

$$\frac{d}{dr} \left( \frac{\delta p}{\rho} \right) = b \left( \frac{\delta p}{\rho} \right). \quad (34)$$

When the argument of the square root in eq. (32) is negative, the wave is evanescent and we enforce the ‘‘hydrostatic’’ boundary condition in eq. (31).

#### 5.1. Zero-frequency limit: the equilibrium tide

The equilibrium tide solution is found by setting  $\sigma \rightarrow 0$  (e.g. Goldreich & Nicholson 1989). The pressure perturbation is found from eq. (25) to be

$$\delta p^{(\text{eq})} = -\rho U. \quad (35)$$

Substitution of eq. (35) into eq. (26) gives

$$\frac{\delta \rho^{(\text{eq})}}{\rho} = \frac{d \ln \rho}{dr} \left( \frac{U}{g} \right). \quad (36)$$

Inserting eq.(35) and eq. (36) into eq. (29) gives

$$N^2 \xi_r = -\frac{N^2}{g} U - g \rho_s \frac{\Delta s}{c_p}. \quad (37)$$

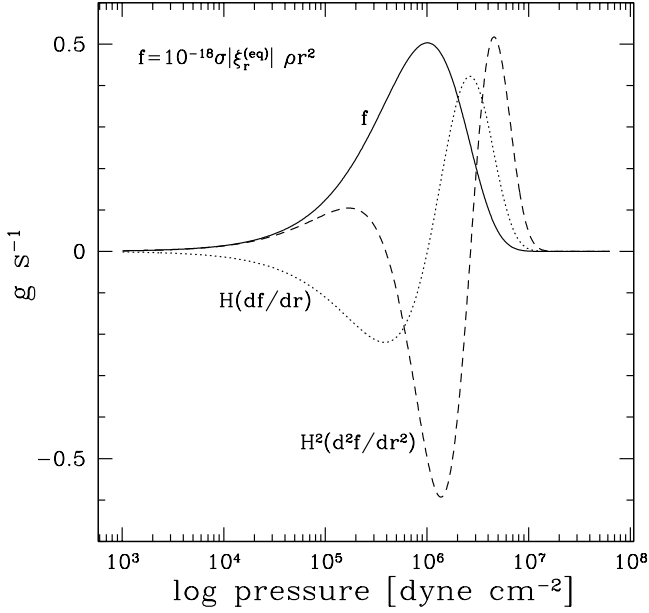


FIG. 3.— Plot of the function  $f = 10^{-18}\sigma|\xi_r^{(\text{eq})}|\rho r^2 = 10^{-18}\rho r^2 \frac{g}{N^2} \frac{\kappa_* F_*}{c_p T} e^{-\kappa_* p/g}$  and its first and second derivative versus depth. Here  $H = p/(\rho g)$  is the pressure scale height. The first derivative is needed for the horizontal displacement (eq.41). In this plot, the base of the heating layer is at  $g/\kappa_* = 1$  bar and the base of the radiative zone is at  $p_b = 100$  bar.

In stably stratified regions,  $N^2 > 0$  and eq. (37) can be solved for the vertical displacement

$$\xi_r^{(\text{eq})} = -\frac{U}{g} - \frac{g}{N^2} \rho_s \frac{\Delta s}{C_p}. \quad (38)$$

In the central convection zone, where  $N^2 \simeq 0$ , no solution exists for eq. (37), since the terms with  $N^2$  go to zero while the  $\Delta s$  term is nonzero. It follows that the concept of an equilibrium tide breaks down in regions that are neutrally stratified and therefore, the forcing frequency cannot be safely set to zero. That is, the fluid response in neutrally stratified regions is inherently a “non-equilibrium tide.” Finally, substitution of eq.(35), (36) and (38) into eq. (27) yields the equilibrium horizontal displacement

$$r\rho\xi_h^{(\text{eq})} = \frac{1}{\ell(\ell+1)} \left[ \frac{d}{dr} \left( r^2 \rho \xi_r^{(\text{eq})} \right) + r^2 \delta\rho^{(\text{eq})} \right]. \quad (39)$$

Hence both vertical and horizontal motions exist in the equilibrium tide limit, driven by gravity and entropy fluctuations.

Clearly, the equilibrium tide density perturbation in eq. (36), and thus the equilibrium tide quadrupole moment, has no contribution from time-dependent surface heating. Inspection of eq. (29) show that the terms  $\propto \Delta s$  cancel out one another. The last term in eq. (29) represents a density decrease due to heating, which is precisely compensated by the  $N^2 \xi_r/g$  term that results from moving across surfaces of constant pressure. In other words, denser fluid is brought up from below, exactly canceling the local density decrease due to heating.

Time-dependent insolation heats the surface and initiates horizontal motion. Consider subsynchronous rota-

tion ( $n - \Omega > 0$ ) so that an observer at rest with respect to the planet sees the star rotate with angle  $\Phi(t) = (n - \Omega)t$  in the positive  $\phi$  direction (see figure 1). For  $m = 2$ , the heating function  $\delta\epsilon \propto \cos[2(\phi - \Phi)]$ , and maxima in the heating function occur at  $\phi - \Phi = 0, \pi$ . The entropy perturbation takes the form (eq.12)

$$\Delta s(\mathbf{x}, t) = \left( \frac{-1}{n - \Omega} \right) \left( \frac{\kappa_* F_*}{c_p T} e^{-\kappa_* p/g} \right) \times Y_{22}(\theta, 0) \sin[2(\phi - \Phi)], \quad (40)$$

giving the hottest points ( $\Delta s$  a maximum) at  $\phi - \Phi = -\pi/4, 3\pi/4$ , and the coldest points at  $\phi - \Phi = \pi/4, -3\pi/4$ . This phase shift reflects the lag between maximum heating and maximum temperature. The displacement in the  $\phi$  direction becomes (eq.39)

$$\xi_\phi(\mathbf{x}, t) = (-1) \left( \frac{1}{n - \Omega} \right) \left( \frac{1}{3r\rho} \right) \times \frac{d}{dr} \left( r^2 \rho \frac{g}{N^2} \frac{\kappa_* F_*}{c_p T} e^{-\kappa_* p/g} \right) \times Y_{22}(\theta, 0) \cos[2(\phi - \Phi)]. \quad (41)$$

The quantity in parenthesis and its derivatives are shown in figure 3. It varies mainly as  $p \exp(-\kappa_* p/g)$ , which has a sharp maximum near the base of the heating layer at  $p = g/\kappa_*$ . Above the base, this derivative is negative and  $\xi_\phi(\phi) \propto \cos[2(\phi - \Phi)]$  describes motion away from regions of high entropy, and toward regions of low entropy. Were there no return flow, mass would accumulate at  $\phi - \Phi = \pi/4, -3\pi/4$ , leading the star. For mass “bumps” leading the star, the quadrupole moment would act to decrease the planet’s spin, pushing it further from synchronous spin. However, there is a return flow, since below the base the direction of  $\xi_\phi$  reverses (see sign of  $df/dr$  in figure 3). As a result, there is no mass accumulation, the density perturbation is identically zero, and there is no net quadrupole. What is required to drive asynchronous spin is a net flow, integrated over depth, away from the the hottest points in the atmosphere.

## 5.2. Finite frequency correction

In this section we derive an analytic expression for the density perturbation due to thermal forcing by using perturbation theory in powers of the frequency. While instructive, this limit is only applicable when resonances with internal waves are unimportant, i.e. at forcing periods  $\ll 1$  day or  $\gg 1$  month.

Let  $\delta p$  and  $\xi_r$  denote the complete solution including both the  $\sigma = 0$  equilibrium tide and the finite frequency corrections. To first order in  $\sigma^2$ , conservation of horizontal momentum gives

$$\delta p = -\rho U + \sigma^2 r \rho \xi_h^{(\text{eq})} = \delta p^{(\text{eq})} + \sigma^2 r \rho \xi_h^{(\text{eq})}. \quad (42)$$

Substituting eq.42 into eq. (26) allows us to write the density perturbation as

$$\delta\rho \simeq \delta\rho^{(\text{eq})} + \frac{\sigma^2}{g} \left[ \rho \xi_r^{(\text{eq})} - \frac{d}{dr} \left( r \rho \xi_h^{(\text{eq})} \right) \right]. \quad (43)$$

For now, we ignore the tidal potential  $U$  and use eq. (39) to write

$$\delta\rho = \frac{\sigma^2}{g} \left[ \rho \xi_r^{(\text{eq})} - \frac{1}{\ell(\ell+1)} \frac{d^2}{dr^2} \left( r^2 \rho \xi_r^{(\text{eq})} \right) \right]. \quad (44)$$

This equation shows that finite fluid inertia effects, scaling as  $\sigma^2$ , give rise to a nonzero density perturbation and consequently, a quadrupole moment.

Attempts to directly integrate eq. (44) lead to numerical difficulties due to the second derivative term, which oscillates with depth. To the extent that  $r^{2+\ell}/g$  is constant, this expression gives a perfect derivative, and the integral would depend only on the endpoints at the center and surface of the planet, where the integrand is negligible. In Appendix A, we show that integration by parts and use of the equations of motion can be used to obtain a more monotonic integrand with significantly less cancellation error.

The expression in eq. (A3) can be estimated analytically in the low frequency limit. If we ignore the  $\delta\rho \propto \sigma^2$  term, substitute eq. (38) for  $\xi_r$  and treat the interior mass  $m(r) \simeq M_p$  as a constant, we find

$$Q = \left( \frac{(4+\ell)(3+\ell)}{\ell(\ell+1)} - 1 \right) \int_0^R dr \rho r^{2+\ell} \frac{\sigma^2}{N^2} \rho_s \frac{\Delta s}{c_p}. \quad (45)$$

This formula directly gives the quadrupole moment in terms of the applied entropy perturbation. Note that the  $\ell$ -dependent prefactor is equal to 4 for  $\ell = 2$ , and vanishes as  $\ell \rightarrow \infty$ .

By comparison, Gold & Soter (1969) assumed constant pressure and ignored vertical motion to obtain a density perturbation  $\delta\rho/\rho = -\delta T/T = -\Delta s/c_p$  (for  $\rho_s = -1$ ).<sup>4</sup> This gives the quadrupole moment

$$Q^{(GS)} = \int_0^R dr \rho r^{2+\ell} \rho_s \frac{\Delta s}{c_p}. \quad (46)$$

The integrand in eq. (45) has the same sign as that of eq. 46, implying a torque which generates asynchronous spin, but suffers a reduction relative to their expression by a factor

$$\left( \frac{(4+\ell)(3+\ell)}{\ell(\ell+1)} - 1 \right) \frac{\sigma^2}{N^2}. \quad (47)$$

As we will see, our numerical solutions to the boundary value problem asymptote to the expression in eq. (45) at long forcing periods.

### 5.3. numerical results

In this section we present numerical results for the solution of eq.(26), (28) and (29) for  $\delta p$ ,  $\delta\rho$  and  $\xi_r$ . To solve these equations, we finite difference in radius with second order accuracy, and write the resulting inhomogeneous equation in matrix form as  $Mx = B$ , where  $M$ ,  $x$  and  $B$  denote the differential operators, solution vector ( $\delta p$ ,  $\delta\rho$  and  $\xi_r$  as a function of radius), and forcing vector (involving  $U$  and  $\Delta s$ ). We find the solution of this linear system using a band-diagonal solver. The quadrupole moment is then evaluated using eq. (A3).

Figure 4 shows the quadrupole moment  $Q_{22}(\sigma)$  as a function of forcing frequency  $\sigma$  for the standard boundary condition in eq. (31). Forcing is solely by  $\Delta s$ , i.e.  $U = 0$ . The parameters used are  $M_p = 0.7M_J$ ,  $R_p = 1.3R_J$ ,  $a = 0.05$  AU, a solar-type star, base of the heating layer at  $g/\kappa_* = 1$  bar and base of the radiative

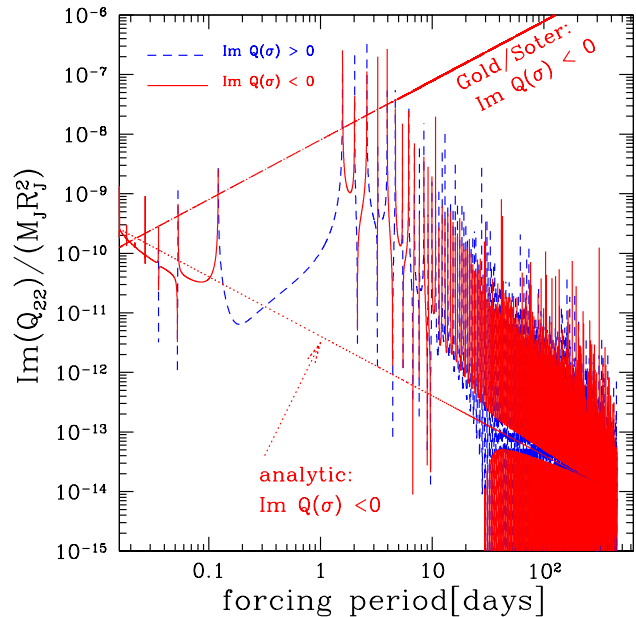


FIG. 4.— Imaginary part of the  $\ell = m = 2$  quadrupole moment as a function of forcing period  $2\pi/\sigma = \pi/(n - \Omega)$ . The quantity  $|Im(Q_{22}(\sigma))|$  is plotted, and short-dashed blue (solid red) lines show positive (negative) values. For comparison, the approximation of Gold & Soter (1969) is shown as the red dot-long dash line, while the approximation in eq. (45) is shown as the red dotted line. The peaks are due to resonances with normal modes of oscillation, with g-modes at long period and f-p modes at short period. The base of the heating layer is at pressure  $g/\kappa_* = 1$  bar, and the base of the radiative zone is at  $p_b = 100$  bar. The solid red lines imply a torque pushing the planet away from synchronous spin, and visa versa for the short-dashed blue lines.

zone at  $p_b = 100$  bar. The absolute value of the imaginary part is plotted. The sign is shown by the line type, solid red line for  $Im(Q_{22}(\sigma)) < 0$ , and dashed blue for  $Im(Q_{22}(\sigma)) > 0$ . The positive forcing frequencies used imply sub-synchronous rotation. Torque has the same sign as  $Im(Q_{22})$ , so that  $Im(Q_{22}) < 0$  drives the planet further from the synchronous state, and vice versa. It is immediately apparent that the response to thermal forcing is dominated by the low order g-modes at periods  $2\pi/\sigma \simeq 1 - 30$  days. This is in contrast to the gravitational tide, which has the largest response for the f-mode at  $2\pi/\sigma \simeq 0.1$  days. Consequently, *the equilibrium tide limit does not apply until the frequency is well below the periods of low order g-modes*. In other words, the low frequency limit of §5.2 is not a good approximation until periods  $2\pi/\sigma > 30$  days for the model shown, rather than  $2\pi/\sigma \sim 0.1$  days, as one would suspect for the gravitational tide.

For comparison, figure 4 shows the GS approximation in eq.46 and the finite frequency correction to the equilibrium tide given by eq. (45). The amplitude at the resonances is set by the frequency spacing used to make the plot; for finer frequency spacing the peaks would be larger. The solution asymptotes to eq. (45) for forcing periods much longer than the low order g-modes. In the range 1-30 days, the quadrupole moment is much larger than the value given by eq. (45), even midway between resonances. The torque alternates sign across some resonances, but not others. For short forcing periods  $\sim 0.1 - 1$

<sup>4</sup> It is unclear if Gold & Soter (1969) assume  $\delta p = 0$  or  $\Delta p = 0$ .

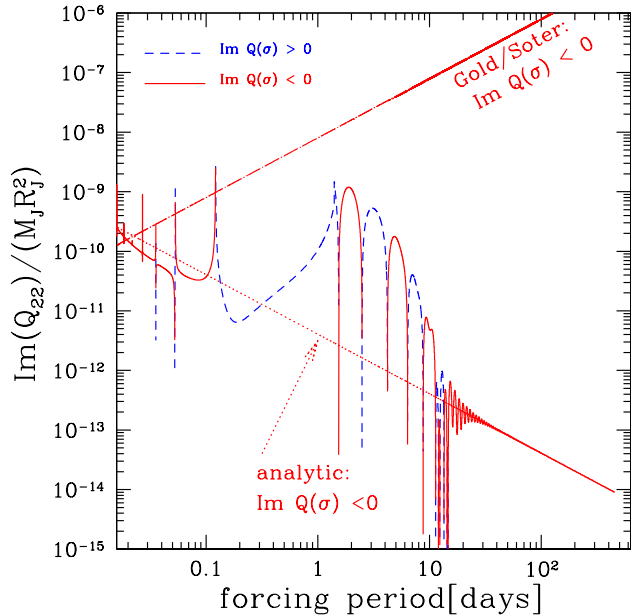


FIG. 5.— Same as figure 4 but with an outgoing wave boundary condition at the upper boundary.

day, the torque acts to synchronize the spin, reinforcing the dissipative gravitational tide torque. However, in between the two lowest order g-modes, at periods  $\simeq 1 - 2$  days, the thermal tide torque is large and acts to torque the planet away from a synchronous spin state.

The sharp peaks in figure 4 are due to resonant response. In the absence of damping, the energy of a standing wave diverges (in linear theory) as the resonance is approached. This is due to the fact that waves can reflect back and forth in the resonant cavity, continually being pumped by the forcing. A second limit one can imagine is that waves with sufficiently short wavelengths at the top of the atmosphere (above the photosphere) propagate upward, carrying away their energy. Figure 5 shows the results for the same parameters as in figure 4, the only modification being the upper boundary condition. Again, there is no forcing by the gravitational tide ( $U = 0$ ). The outgoing wave boundary condition has eliminated the sharp resonances for high order g-modes. The exact numerical response agrees well with the analytic formula in eq. (45) beyond a forcing period of 1 month. For the important period range 1 day-1 month, the quadrupole moment is again 1-3 orders of magnitude larger than expected from the analytic formula, due to the response of low order g-modes – *even for the leaky upper boundary*. As we show in the next section, this enhanced response is due to the good overlap of gravity waves with the thermal forcing.

## 6. OVERLAP OF OSCILLATION MODES WITH THERMAL AND GRAVITATIONAL FORCING

At forcing periods  $> 1$  month, the frequency dependent quadrupole moment asymptotically approaches the analytic result in eq. (45), derived by treating fluid inertia as a small correction to the equilibrium tide solution. However, the range of forcing periods of interest in determining asynchronous rotation of hot Jupiters is likely  $\lesssim 1$  month. In this range of forcing periods, low

radial order gravity waves propagate in the radiative envelope and even the off-resonant response of these waves increases the quadrupole moment by 1-3 orders of magnitude compared to eq. (45). In what follows, we show that the forced entropy fluctuations may be understood as an external force that is exerted upon the planetary fluid. Given the expression for this force, the standard machinery developed for the purpose of understanding dynamic gravitational tides (Cowling 1941; Zahn 1970, 1975; Press & Teukolsky 1977; Goldreich & Nicholson 1989) can be applied to the thermal forcing case in order to understand the corresponding quadrupole moments.

### 6.1. Forced Oscillator Formalism

The fluid fluctuations in the planet can be thought of as a forced oscillator that obeys

$$\ddot{\boldsymbol{\xi}} + \mathbf{C} \cdot \boldsymbol{\xi} = -\mathbf{D} \cdot \dot{\boldsymbol{\xi}} + \mathbf{a} \quad (48)$$

where  $\mathbf{C}$  is a self-adjoint operator, responsible for the adiabatic restoring forces (Lynden-Bell & Ostriker 1967) and  $\mathbf{a} = \mathbf{a}^G + \mathbf{a}^S$  is the sum of the gravitational tidal force

$$\mathbf{a}^G = -\nabla U \quad (49)$$

and the force due to time-dependent insolation,  $\mathbf{a}^S$ . We have also added an ad hoc damping term  $\mathbf{D} \cdot \dot{\boldsymbol{\xi}}$ . To compute the form of  $\mathbf{a}^S$ , the pressure and buoyancy forces in eq. (26) must be expressed in terms of  $\boldsymbol{\xi}$  using eq. 20 and 29 using

$$\begin{aligned} \delta p &= \rho c^2 \left( \frac{\delta \rho}{\rho} - \frac{N^2}{g} \xi_r - \rho_s \frac{\Delta s}{c_p} \right) \\ &= -c^2 \left( \nabla \cdot (\rho \boldsymbol{\xi}) + \rho \frac{N^2}{g} \xi_r + \rho \rho_s \frac{\Delta s}{c_p} \right). \end{aligned} \quad (50)$$

Terms involving  $\boldsymbol{\xi}$  combine to give  $\mathbf{C} \cdot \boldsymbol{\xi}$ . The total pressure force contains a non-adiabatic term that results from time-dependent insolation, which we identify as

$$\mathbf{a}^S = \frac{1}{\rho} \nabla \cdot \left( \rho c^2 \rho_s \frac{\Delta s}{c_p} \right) \quad (51)$$

The entropy fluctuation  $\Delta s$  is specified by eq. (10).

The externally forced fluid displacement  $\boldsymbol{\xi}$  can be decomposed into the free adiabatic eigenmodes  $\boldsymbol{\xi}_\alpha$  as

$$\boldsymbol{\xi}(\mathbf{x}, t) = \sum_{\alpha} q_{\alpha}(t) \boldsymbol{\xi}_{\alpha}(\mathbf{x}). \quad (52)$$

Here,  $q_{\alpha}(t)$  is the time-dependent eigenmode amplitude. The free adiabatic eigenmodes  $\boldsymbol{\xi}_{\alpha}(\mathbf{x}) e^{-i\sigma_{\alpha} t}$  with eigenfrequency  $\sigma_{\alpha}$  obey

$$-\sigma_{\alpha}^2 \boldsymbol{\xi}_{\alpha} + \mathbf{C} \cdot \boldsymbol{\xi}_{\alpha} = 0. \quad (53)$$

The Hermitian nature of the operator  $\mathbf{C}$  implies that the eigenfunctions obey the orthogonality condition  $\int d^3x \rho \boldsymbol{\xi}_{\alpha}^* \cdot \boldsymbol{\xi}_{\beta} = A_{\alpha\alpha} \delta_{\alpha\beta}$ , where  $\delta_{\alpha\beta}$  is the delta function and  $A_{\alpha\alpha} = \int d^3x \rho |\boldsymbol{\xi}_{\alpha}|^2$ .

By projecting eq. (48) onto mode  $\alpha$  using the orthogonality relation, the amplitude  $q_{\alpha}(t)$  obeys the following forced oscillator equation

$$\ddot{q}_{\alpha} + \sigma_{\alpha}^2 q_{\alpha} = -\gamma_{\alpha} \dot{q}_{\alpha} + \frac{1}{A_{\alpha\alpha}} \int d^3x \rho \boldsymbol{\xi}_{\alpha}^* \cdot \mathbf{a}(\mathbf{x}, t), \quad (54)$$



where  $\gamma_\alpha$  is the damping rate. In general, damping can be due to microphysical process such as viscosity and thermal diffusion. It may also represent the loss of energy at the upper boundary due to the outgoing wave boundary condition, which can also then lead to a broadening of the resonant response. Plugging in a particular harmonic  $\mathbf{a}(\mathbf{x}, t) = \mathbf{a}(\mathbf{x}, \sigma)e^{-i\sigma t}$ , the amplitude of the forced response is given by

$$q_\alpha(\sigma) = \frac{\int d^3x \rho \boldsymbol{\xi}_\alpha^* \cdot \mathbf{a}(\mathbf{x}, \sigma)}{A_{\alpha\alpha}(\sigma_\alpha^2 - \sigma^2 - i\sigma\gamma_\alpha)}. \quad (55)$$

Note that the mode amplitude  $q_\alpha(\sigma)$  can be forced by both tidal gravity, which leads to an in phase response, and the time-dependent insolation, which leads to an out of phase response.

### 6.2. Quadrupole Moment in Terms of Overlap Integrals

The frequency dependent quadrupole moment is found by combining the mode amplitude in eq.55 and the quadrupole moment from eq.19 to find

$$\begin{aligned} Q_{\ell m}(\sigma) &= \sum_\alpha \frac{[\int d^3x \rho \boldsymbol{\xi}_\alpha^* \cdot \mathbf{a}(\mathbf{x}, \sigma)] [\int d^3x \rho \boldsymbol{\xi}_\alpha \cdot \nabla (r^\ell Y_{\ell m}(\theta, \phi))]}{A_{\alpha\alpha}(\sigma_\alpha^2 - \sigma^2 - i\gamma_\alpha\sigma)} \\ &= \sum_\alpha Q_{\alpha\ell m}(\sigma) \left( \frac{2\sigma_\alpha^2}{\sigma_\alpha^2 - \sigma^2 - i\gamma_\alpha\sigma} \right) \end{aligned} \quad (56) \quad (57)$$

where we identify the quadrupole moment of mode  $\alpha$  as

$$Q_{\alpha\ell m}(\sigma) = \frac{[\int d^3x \rho \boldsymbol{\xi}_\alpha^* \cdot \mathbf{a}(\mathbf{x}, \sigma)] [\int d^3x \rho \boldsymbol{\xi}_\alpha \cdot \nabla (r^\ell Y_{\ell m}(\theta, \phi))]}{2A_{\alpha\alpha}\sigma_\alpha^2} \quad (58)$$

For forcing frequencies  $\sigma \ll \sigma_\alpha$ , eq.57 shows that  $2Q_{\alpha\ell m}$  can be identified with the quadrupole moment contribution from mode  $\alpha$  at low frequency. Note that  $Q_{\alpha\ell m}$  is a physical quantity, since the normalization factors for the eigenmodes cancel out. Also note that the  $Q_{\alpha\ell m}$  have frequency dependence solely due to  $\Delta s \propto \sigma^{-1}$ . This dependence is factored out by writing

$$\text{Im}[Q_{\alpha\ell m}(\sigma)] = \text{Im}[Q_{\alpha\ell m}(\sigma_\alpha)] \left( \frac{\sigma_\alpha}{\sigma} \right). \quad (59)$$

The imaginary part of the quadrupole moment, which determines the secular torque on the orbit and spin, can be written out as

$$\begin{aligned} &\text{Im}[Q_{\ell m}(\sigma)] \\ &= \sum_\alpha \frac{2\sigma_\alpha^2}{(\sigma_\alpha^2 - \sigma^2)^2 + \gamma_\alpha^2\sigma^2} \\ &\times (\text{Re}[Q_{\alpha\ell m}(\sigma)]\gamma_\alpha\sigma_\alpha + \text{Im}[Q_{\alpha\ell m}(\sigma)](\sigma_\alpha^2 - \sigma^2)). \end{aligned} \quad (60)$$

In the absence of dissipation ( $\gamma_\alpha = 0$ ), the gravitational tide exerts no torque since the response is in phase, and  $\text{Im}[Q_{\alpha\ell m}(\sigma)] = 0$ . Including dissipation ( $\gamma_\alpha \neq 0$ ), the gravitational tide gives rise to a torque due to the first term in eq. (60). By contrast, the thermal tide response is inherently out of phase. Hence even when  $\gamma_\alpha = 0$ , the thermal tide causes a secular torque. Inclusion of damping for the thermal tide will act to prevent divergent response at resonances, due to the denominator of the Lorentzian in eq. (60).

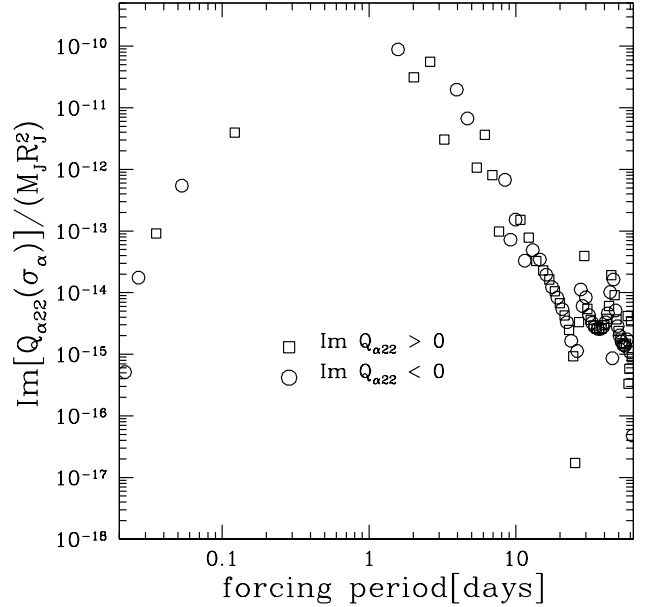


FIG. 6.— Quadrupole moments  $Q_{\alpha 22}$  for the oscillation modes. G-modes have periods longer than 1 day, and f-p modes have periods shorter than 1 day. The plot shows  $Q_{\alpha 22}$  for  $\ell = m = 2$  for each oscillation mode for the sum in eq. (57) for the frequency dependent quadrupole. The base of the radiative zone is at  $p_b = 100$ bar, and the base of the heated layer is at  $g/\kappa_* = 1$ bar. Other parameters are the same as in figure 4. The circles (squares) show modes with  $\text{Im}(Q_{\alpha 22}) < 0$  ( $\text{Im}(Q_{\alpha 22}) > 0$ ). A radial resolution of 9447 grid points was used to compute the results shown in this plot. The results are numerically converged for most of the modes shown even at much lower resolution.

Figure 6 shows the quadrupole moments  $Q_{\alpha 22}(\sigma_\alpha)$  for each mode as defined in eq. (57) and (58) for the same parameters used to find the frequency dependent quadrupole moment in figure 4. These quadrupole moments were computed by fitting the  $Q_{22}(\sigma)$  near resonance using eq. (57) in order to read off the coefficient  $Q_{\alpha 22}(\sigma_\alpha)$ . It is immediately apparent that the dominant overlap is with the lowest order g-mode at period  $\approx 1$  day. The f and p mode quadrupoles are down by 1-2 orders of magnitude.

To verify the equivalence between the solution of the boundary value problem and the sum over eigenmodes, the frequency dependent response  $Q_{22}(\sigma)$  is compared to the sum over eigenmodes from eq. (57) in figure 7. Damping is neglected, i.e. the standard boundary condition in eq. (31) is used. Despite the fact that only a handful of low order g-modes are used in the sum, and that the f and p modes are not included, there is good agreement with the solution to the full boundary value problem.

The difference resulting from the two different upper boundary conditions as shown in figures 4 and 5 can be understood using eq.60. Figure 4 has  $\gamma_\alpha = 0$ , and hence divergences appear in the quadrupole moment near the frequencies of internal standing waves. In figure 5, damping is introduced through the outgoing wave boundary condition. In fact this damping is so large that  $\gamma_\alpha \sim \sigma_\alpha$ , and the Lorentzian factors  $\sigma_\alpha^4 / ((\sigma_\alpha^2 - \sigma^2)^2 + \gamma_\alpha^2 \sigma^2) = \mathcal{O}(1)$ . For Lorentzian factor of order unity, the induced quadrupole moment is of order

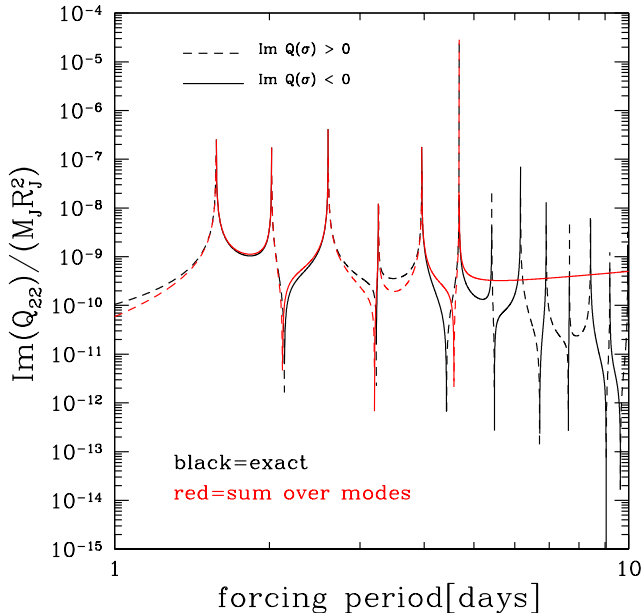


FIG. 7.— Comparison of the numerical response (black lines) versus the sum over modes in eq. 57 and 59 (red lines). The coefficients  $Q_{\alpha 22}(\sigma_\alpha)$  for each mode are shown in figure 6, and the response is for the case shown in figure 4. Only modes in the period range 1-5 days were used to make the red lines; in particular, no f or p modes were used. Note the sum over modes agrees well for low order g-modes, even midway between resonances, implying the off-resonant response of the f and p-modes is weak compared to that of low order g-modes. Agreement could be improved by including additional modes in the sum.

the overlap integral  $Q_{\alpha lm}(\sigma_\alpha)$ .

Even for large damping rates  $\gamma_\alpha \sim \sigma_\alpha$ , the low order g-modes still dominate the response since their overlap integrals with the thermal tide force are far larger than the f and p-modes (see figure 6). In the duration of one wave travel time in the radiative layer, the wave can build up enough energy to dominate the response. The overlap integrals in figure 6 are larger than near-equilibrium tide result from eq. (45) in the period range 1 day - 1 month, precisely the region where enhanced response is seen in figure 5.

The spatial profiles of thermal and gravitational forcing differ greatly from one another. Thermal forcing is localized in physical space to the outer layers of the planet, resembling a delta function in space. By contrast, the gravitational tide most closely resembles the f-mode, and can be thought of as a delta function in momentum space (Reisenegger 1994). In other words, since thermal forcing is narrow in physical space, the fluid response, in terms of normal modes, is broad in momentum space, and visa versa for the gravitational tide. However, the g-modes which propagate within the stably stratified envelope dominate since their frequencies are comparable to forcing frequencies of interest, and their eigenfunctions are confined to the radiative layer where the thermal forcing occurs. The frequencies of f and p-modes are too high to be resonant, and their eigenfunctions extend over the entire planet.

## 7. ON THE NEGLECT OF THE CORIOLIS FORCE, THERMAL DIFFUSION, AND BACKGROUND FLOWS

In an attempt to elucidate the origin of quadrupole moments from thermal forcing, we have made a number of simplifying assumptions so as not to obscure the basic physics. In this section we comment on how our results might be changed, both qualitatively and quantitatively, by relaxing these assumptions.

### 7.1. the Coriolis force

Consider the effect of uniform rotation, with spin frequency  $\Omega$ . When  $\sigma \lesssim \Omega$ , the Coriolis force becomes important for the fluid response and we anticipate several additional effects due its presence. First, the gravity wave dispersion relation and fluid motions are altered. For  $\sigma \sim \Omega$ , we expect the change in the quadrupole to be at the factor of a few level in the “bump” between 1-30 days. Second, new wave families arise, mainly restored by the Coriolis force – the Rossby waves, or inertial waves. These waves can propagate throughout both the radiative envelope and the convective core. We expect that, for sufficiently rapid supersynchronous rotation, Rossby resonances may give rise to a larger quadrupole moment. In the perturbation theory calculation of §5.2, we expect *larger* quadrupole moment when the spin is nearly synchronous, since the Coriolis terms  $\propto \sigma\Omega$  will be larger than the inertia terms  $\propto \sigma^2$ . In figures 4 and 5 this will lead to the “analytic” line becoming flat, instead of decreasing to longer forcing period.

For sufficiently large quadrupole moment, the equilibrium spin will be asynchronous enough that  $\sigma \gtrsim \Omega$ , and we expect our results to be approximately quantitatively correct. Substitution of the quadrupole moment in figure 5 into eq. 4, for  $Q_p = 10^6$  we find  $\sigma \sim n$  in the period range of  $\sim$  a few days, implying the spin frequency, orbital frequency and forcing frequency are all comparable in torque equilibrium. In this event, the Coriolis force is important, but will only change the frequencies and eigenfunctions of the gravity waves at the order unity level.

### 7.2. thermal diffusion

The heating function in eq.11 describes the law of exponential attenuation of stellar radiation. By setting this to occur at a pressure  $\sim 1$  bar, we are assuming there are no absorbers high in the atmosphere. Until recently, this assumption was standard, but there may now be evidence of an inversion layer due to such absorbers in a fraction of observed hot Jupiters (Fortney et al. 2008). In that case, incorporating thermal forcing by the boundary condition used in Gu & Ogilvie (2009) may be more appropriate.<sup>5</sup>

The entropy perturbation in eq.10 assumes that the forcing period is much shorter than the thermal time in the heated layer, so that radiation diffusion may be ignored. In fact, thermal diffusion and damping of downward propagating waves is expected, as in the solutions of Gu & Ogilvie (2009). Furthermore, a shorter diffusion time may partially “erase” temperature perturbations, reducing the buoyancy force upon which gravity waves rely. This may cause wave damping or reflection near the optical or infrared photospheres. By choosing

<sup>5</sup> If one considers a two-frequency, two-angle approximation to the radiative transfer, both the “greenhouse” and the “stratosphere” cases may be included.

the “perfect reflector” and “leaky” upper boundary conditions in section 5.3 we attempted to simulate two extreme limits of the effects of radiative diffusion. While thermal diffusion may decrease the amplitude of gravity waves near the photosphere, deeper in the envelope the thermal time becomes sufficiently long so that damping can be ignored.

For forcing period of order a few days, the thermal time at the base of the heating layer is of order the forcing period. Therefore, the approximation that the layer possesses a large thermal inertia is only approximately valid. Another effect we have ignored is that nonlinear effects become important when the forcing period is longer than the thermal time.

### 7.3. fluid flow in the background state

We now comment on the possible role of fluid motion such as zonal flows in the background state. Fluid motion in the background state does not preclude the existence of the gravity (or inertial) wave response as described in this paper. Ignoring shearing of the velocity field, such a flow would simulate uniform rotation, so that the Coriolis force becomes important. However, when there is velocity shear in the background state, we expect the wave motions to be significantly modified when the shear rate is comparable to the wave frequency. Since inertial wave response relies on angular momentum gradients, we expect these waves to persist in the presence of velocity shear. Most atmospheric circulation simulations for the hot Jupiters (e.g. Dobbs-Dixon & Lin 2008, Showman et al. 2009) assume synchronous rotation, and find powerful advective flows. Relatively few simulations with asynchronous rotation have been performed, but the recently results by Showman et al. (2009) are useful in this context. They found that when the degree of asynchronous spin was increased, the flow velocities were decreased. It remains to be seen what winds are induced for rotation rates appropriate for the torque equilibrium described in section 2. All current studies of atmospheric circulation in hot Jupiters ignore the thermal tide torques. From the analysis presented in this work, it seems likely that the qualitative and quantitative outcome of these simulations will change once thermal tidal torques are included.

## 8. SUMMARY

We considered the ability of a planet, subjected to time-dependent stellar irradiation, to develop net quadrupole moments. The existence of such quadrupole moments allows the stellar tidal field to exert torques on the planet, possibly creating asynchronous spin. Such asynchronous spin could lead to large tidal heating rates, through the dissipative gravitational tide, perhaps sufficient to power the large observed radii.

In §5.1 and 5.2, the fluid equations are solved treating inertia as a small parameter. At zeroth order in the forcing frequency, a circulation pattern is found from hot to cold at small depths  $p \lesssim g/\kappa_*$ , and a return flow from cold to hot at larger depth  $p \gtrsim g/\kappa_*$ . There is no density perturbation associated with this flow and there-

fore, zero quadrupole moment. The inclusion of finite inertia as a small perturbation gives rise to a finite density perturbation and therefore, quadrupole moment. In the assumed limit of small fluid inertia, the phase of the quadrupole is found to have the correct sign to induce asynchronous rotation in the planet, similar to the work of Gold & Soter (1969). However, the magnitude of this quadrupole is reduced by a factor  $\sim 4(\sigma/N)^2$ . A propagating wave-like response of any form is eliminated in this “near-equilibrium tide” approximation. The value of the resulting quadrupole moment is insensitive to boundary conditions and depends solely on the local forcing in the atmosphere. Numerical calculations presented in figure 4 and 5 confirm that the quadrupole moment approaches this analytic limit at long forcing periods.

In §5.3, the fluid equations are solved as a boundary value problem. Two different upper boundary conditions are used, which effectively treat the radiative envelope as a perfect resonant cavity, or as a cavity with an open upper lid, allowing waves to be radiated upward. Using both boundary conditions, which may bracket the true result including radiative transfer effects, it is found that the quadrupole moments in the period range 1 day - 1 month are far larger than the non-resonant near-equilibrium tide calculation in eq. 45 by 1-3 orders of magnitude. The reason for this enhanced response is discussed in §6. Unlike the gravitational tidal forcing, time-dependent thermal forcing and low order envelope g-modes couple well due a favorable spatial overlap.

In section 2, we argued that the magnitude of the thermal tide torques using the formula of Gold & Soter (1969) is sufficient to generate large deviations from synchronous rotation as well as large tidal heating rates, easily sufficient to power the observed planet radii. Our numerical results in §5.3 show that the full numerical solutions for the torque can indeed have the correct sign to generate asynchronous spin for some ranges of forcing (rotation) frequency. The magnitude of the torques is smaller than the Gold & Soter (1969) result by a factor of a few, but still large enough to be interesting. We expect that the inclusion of the Coriolis force will *increase* the torque at long forcing periods, since the Coriolis force is larger than fluid inertia in that limit.

In future investigations, we plan on including the effects of the Coriolis force and thermal diffusion in the calculation of the quadrupole moments. We expect that both physical effects could lead to qualitative and quantitative changes to the non-resonant and resonant thermal tidal response. The resulting torques will then be used to solve for the equilibrium values of the planet’s spin, radius and eccentricity.

We thank Peter Goldreich for helpful discussions. Also, we thank Jeremy Goodman, Gordan Ogilvie and Pin-Gao Gu for raising the issue of isostatic adjustment as well as Yanqin Wu for discussions of the upper boundary condition. We also thank the referee for comments that improved the paper.

## APPENDIX

## ACCURATE EVALUATION OF THE QUADRUPOLE MOMENT: INTEGRATION BY PARTS

As discussed in section 5.2, direct integration of  $r^\ell \delta\rho$  to find the quadrupole moment is subject to large cancellation errors. This behavior is somewhat surprising, and does not occur for the gravitational tide quadrupole moment. The origin of the problem is that  $\delta\rho$  is proportional to the second derivative of a certain quantity, resulting in large cancellations during the integration. We noticed this cancellation error during numerical resolution studies in which the results did not converge rapidly with increasing resolution.

Here, we show that this cancellation error can be ameliorated through successive integration by parts, and use of the equations of motion. By using the exact equations of motion, this method does not introduce approximations. Integration by parts leads to an integrand that is much more monotonic, leading to better convergence.

The quadrupole moment is given by

$$Q = \int_0^R dr r^{2+\ell} \delta\rho. \quad (\text{A1})$$

By substituting for  $\delta\rho$  from eq. (26) gives

$$Q = \int_0^R dr r^{2+\ell} \frac{\rho}{g} \left( \sigma^2 \xi_r - \frac{1}{\rho} \frac{d\delta p}{dr} - \frac{dU}{dr} \right). \quad (\text{A2})$$

Integrating the pressure gradient term by parts, discarding the (small) boundary terms, and solving eq.28 for  $\delta p$ , we find

$$Q = \int_0^R dr r^{2+\ell} \frac{\rho}{g} \left( \sigma^2 \xi_r - \frac{dU}{dr} \right) + \frac{\sigma^2}{\ell(\ell+1)} \int_0^R dr \frac{d}{dr} \left( \frac{r^{2+\ell}}{g} \right) \left[ r^2 \delta\rho + \frac{d}{dr} (r^2 \rho \xi_r) - \frac{\ell(\ell+1)}{\sigma^2} \rho U \right].$$

Integrating the  $d/dr(r^2 \rho \xi_r)$  term by parts and simplifying gives the final result

$$Q = \int_0^R dr r^{2+\ell} \delta\rho^{(\text{eq})} + \sigma^2 \int_0^R dr \left[ \rho \xi_r \left\{ \frac{r^{2+\ell}}{g} - \frac{r^2}{\ell(\ell+1)} \frac{d^2}{dr^2} \left( \frac{r^{2+\ell}}{g} \right) \right\} + \frac{r^2}{\ell(\ell+1)} \frac{d}{dr} \left( \frac{r^{2+\ell}}{g} \right) \delta\rho \right]. \quad (\text{A3})$$

The first term in eq. (A3) is just the equilibrium  $\sigma^2 = 0$  quadrupole from gravitational forcing alone – see eq. (36). Although the  $\delta\rho$  term in eq. (A3) may be subject to cancellation error, this term should be smaller by a factor  $\sigma^2 r/g$  compared to the other terms after integration. Since the equilibrium tide component of  $\xi_r$  is monotonic, the terms involving  $\xi_r$  do not suffer cancellation error. We find numerically that integrand is far more monotonic than  $r^{2+\ell} \delta\rho$ , and is less subject to cancellation error. Throughout, we use eq. (A3) when numerically evaluating the quadrupole moment that results from thermal forcing.

## REFERENCES

- Arras, P., & Bildsten, L. 2006, ApJ, 650, 394  
 Burrows, A., Guillot, T., Hubbard, W. B., Marley, M. S.,  
 Saumon, D., Lunine, J. I., & Sudarsky, D. 2000, ApJ, 534, L97  
 Cowling, T. G. 1941, MNRAS, 101, 367  
 Dobbs-Dixon, I., & Lin, D. N. C. 2008, ApJ, 673, 513  
 Fortney, J. J., Lodders, K., Marley, M. S., & Freedman, R. S.  
 2008, ApJ, 678, 1419  
 Gold, T., & Soter, S. 1969, Icarus, 11, 356  
 Goldreich, P., & Kumar, P. 1990, ApJ, 363, 694  
 Goldreich, P., & Nicholson, P. D. 1989, ApJ, 342, 1079  
 Goldreich, P., & Soter, S. 1966, Icarus, 5, 375  
 Goodman, J. 2009, arXiv:0901.3279  
 Gu, P.-G., & Ogilvie, G. I. 2009, MNRAS, 395, 422  
 Newcomb, W. A. 1962, Nuclear Fusion: Supplement Part 2,  
 Vienna: International Atomic Energy Agency, 451.  
 Press, W. H., & Teukolsky, S. A. 1977, ApJ, 213, 183  
 Reisenegger, A. 1994, ApJ, 432, 296  
 Showman, A. P., Fortney, J. J., Lian, Y., Marley, M. S.,  
 Freedman, R. S., Knutson, H. A., & Charbonneau, D. 2009,  
 ApJ, 699, 564  
 Unno, W., Osaki, Y., Ando, H., Saio, H., & Shibahashi, H. 1989,  
 Nonradial oscillations of stars, Tokyo: University of Tokyo  
 Press, 1989, 2nd ed.,  
 Zahn, J. P. 1970, A&A, 4, 452  
 Zahn, J.-P. 1975, A&A, 41, 329